Journal of Solid State Chemistry **148,** 169–177 (1999)
Article ID jssc.1999.8495, available online at http://www.idealibrary.com on IDEAL®

Giant Haven Ratio for Proton Transport in Sodium Hydroxide

M. Spaeth, K. D. Kreuer, and J. Maier

Max-Planck-Institut für Festkörperforschung, 70569 Stuttgart, Germany

and

C. Cramer

Westfälische Wilhelms-Universität, Institut für Physikalische Chemie, 48149 Münster, Germany

Received April 22, 1999; in revised form August 31, 1999; accepted September 7, 1999

Solid sodium hydroxide has been prepared and investigated with respect to its transport properties. The proton conductivity depends significantly on the water content. In NaOH with minimum water content (NaOH in phase equilibrium with Na_2O) the proton conductivity is much lower than reported in the literature. Defect chemistry and transport characteristics are discussed. For the same dry samples pulsed field gradient NMR revealed a surprisingly high H-diffusion coefficient and thus a Haven ratio of $10-10^4$ in the cubic phase. In fact this value is only the lower limit since the measured conductivity may still be influenced by residual extrinsic effects or due to Na^+ contributions. A cooperative mechanism is described which is able to explain this anomaly. © 1999 Academic Press

Key Words: **proton conductivity; tracer diffusion; correlations; sodium hydroxide.**

INTRODUCTION

In contrast to the well-known proton conducting oxides, in which H_2O can be dissolved under formation of internal OH-groups, according to

$$H_2O + O_O^{\times} + V_O^{\cdot\cdot} \rightleftharpoons 2OH_O^{\bullet}, \qquad [1]$$

OH^- is the major anionic constituent in hydroxides. In proton conducting oxides the $OH\cdots O$ distance is small enough to easily enable a Grothuss-type of H^+ migration. By contrast, the O–O distance in the high-temperature phase of the alkaline metal hydroxides is too large (360–460 pm) to support this kind of transport mechanism. Also the amphoteric nature of OH^- is probability not marked enough to facilitate a proton donor–acceptor mechanism, nor does it—in contrast, e.g., to the high temperature phase of $CsHSO_4$ (1)—favor a pronounced self-dissociation of OH^- into internal HOH and O^{2-}. However, the high proton density should lead to the possibility of cooperative motion. Haas and Schindewolf (2, 3), Stephen and Howe (4) and Élk'kin *et al.* (5, 6) found enormously (but different) high conductivity values (7, 8). While the former authors explained this in terms of water and carbonate contaminations, the latter ones held the above-mentioned autoprotolysis reaction responsible for the significant conductivity. In the following paper we investigate proton transport with two alternative methods, impedance spectroscopy and pulsed field gradient NMR (PFG-NMR). Special emphasis is laid on the preparation of pure, water-free NaOH (see Ref. (7, 8)). A general report on our measurements of the hydroxides of the alkaline group (besides NaOH also KOH, RbOH, and CsOH) has already been given elsewhere (9). This paper focuses on NaOH and is much more detailed with respect to defect chemistry and transport.

In the high-temperature cubic phase of NaOH the anisotropic OH^- ions are fully rotationally disordered, a freezing of which leads to a symmetry reduction. Besides the cubic rock salt structured phase ($560\ K < T < T_{melt} = 592\ K$), NaOH exhibits a monoclinic phase ($514\ K \leq T \leq 566\ K$) and below 514 K an orthorhombic phase. A detailed description of the structure can be found in Refs. (7, 10–17) (see Fig. 1). Before we discuss the experimental results let us consider the expected defect chemical situation.

DEFECT CHEMISTRY OF HYDROXIDES

In addition to the ionic disorder reactions which we usually discuss in compounds with elemental cations and anions (M^+X^-), e.g,. Frenkel-, Anti-Frenkel-, Schottky-, and Anti-Schottky-disorder describing spatial displacement processes of anions and cations, in compounds exhibiting a "complex" ion, such as the anion OH^-, we face also the possibility of compositional disorder within a single ion (i.e.,

0022-4596/99 $30.00

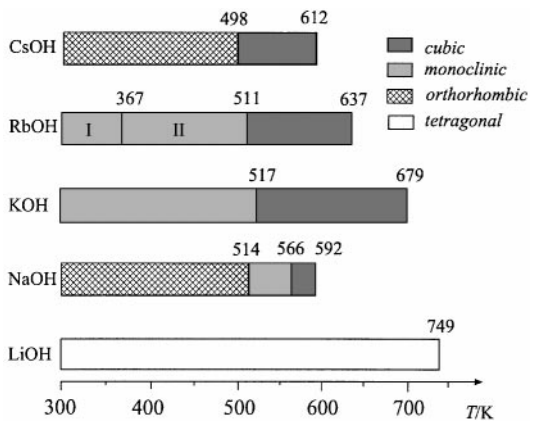

FIG. 1. Survey of the modifications occurring in the alkaline metal hydroxides (18).

O^{2-} or H_2O instead of OH^-). In the cases of the hydroxides this refers to the above-mentioned autoprotolysis reaction

$$2OH_{OH}^{\times} \rightleftharpoons H_2O_{OH}^{\bullet} + O_{OH}'. \qquad [2]$$

Electronic processes are unlikely to occur in NaOH to a major extent. A relatively plausible redox reaction might be the formation of peroxide defects ($O^- \triangleq O_{OH}^{\times}$)

$$\tfrac{1}{2}O_2 + 2OH_{OH}^{\times} \rightleftharpoons H_2O + 2O_{OH}^{\times} \rightleftharpoons H_2O + 2h^{\bullet} + 2O_{OH}'. \qquad [3]$$

Yet, there are no indications of electronic contributions to the conductivity nor have we found any traces of paramagnetic centers by EPR (detection limit 10^{12} spins/cm^3, see below). So in fact, as we shall see, the part usually played by the electronic carrier in the Kröger–Vink diagrams is "taken over" by the protonic defects. A water excess over the intrinsic value (denoted by $[H_2O]^*$) can be incorporated in the form of interstitial OH^-(OH_i') accompanied by a protonation of regular OH^- (formation of $H_2O_{OH}^{\bullet}$ or $H_2O_i^{\times}$):

$$H_2O + OH_{OH}^{\times} + V_i \rightleftharpoons OH_i' + H_2O_{OH}^{\bullet} (\rightleftharpoons H_2O_i + OH_{OH}^{\times}). \qquad [4]$$

Thus in the H_2O-rich ($[H_2O] > [H_2O]^*$) branch the hydroxide is comparatively acidic.

This will be the decisive mode of incorporation if OH^- can occupy interstices in the structure. In this case we expect an Anti-Frenkel reaction to be important

$$OH_{OH}^{\times} + V_i \rightleftharpoons V_{OH}^{\bullet} + OH_i'. \qquad [5]$$

The other possibility is Anti-Schottky disorder which also involves OH_i' but also the formation of $Na_i^{\bullet}$. This is a very unusual disorder mode but may not be completely excluded in view of the loose structure. If only Schottky disorder

$$OH_{OH}^{\times} + Na_{Na}^{\times} \rightleftharpoons V_{OH}^{\bullet} + V_{Na}' + NaOH \qquad [6]$$

were possible, the water solubility would be restricted to the filling of the OH^- vacancies and thus to small values. NaOH is, however, known to absorb as much as several percent of water as will be discussed below (Ref. (19)). In principle, however, the water solubility may consist of a formation of a water excess and/or an annihilation of a water deficiency formed according to

$$2OH_{OH}^{\times} \rightleftharpoons H_2O + V_{OH}^{\bullet} + O_{OH}'. \qquad [7]$$

In this branch the hydroxide is comparatively basic. What we definitely know is that the equilibrium homogeneity range is bounded by the phase equilibrium with Na_2O on one side and $NaOH \cdot H_2O$ on the other side.

Figure 2 shows the equilibrium partial pressure of water as a function of the H_2O/Na_2O ratio at 336 K as calculated from Ref. (20). The course inside the single phase regimes is not known.

Figure 3 shows the native disorder in the hydroxides in form of Kröger–Vink diagrams. We recognize the similiarity to the usual diagrams for pure oxides if we replace the role of electrons by the role of protons. Use has been made of the electroneutrality assumption and of the equilibria for the reactions described by Eqs. [2], [4], and [5] (Eq. [7] is redundant), i.e., an Anti-Frenkel disorder has been assumed to dominate the ionic disorder. It can be immediately deduced from the diagrams that the proton conductivity is expected to increase in the H_2O-excess region while it is expected to decrease in the H_2O-deficient region unless the

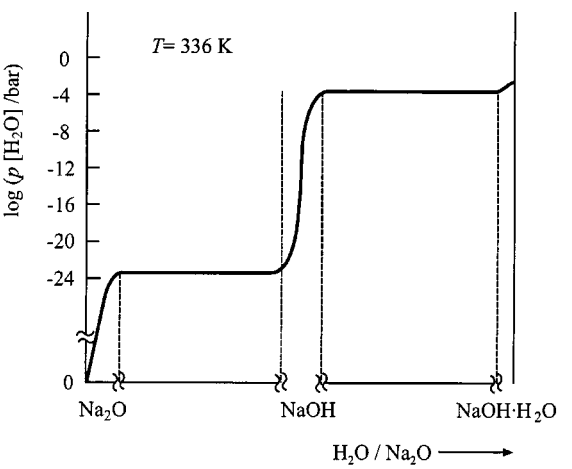

FIG. 2. Equilibration partial pressure of water in the relevant section of the system Na_2O–H_2O. The course within the phases is schematic (18). As will be discussed below, the point of inflection within the NaOH phase will be close to the left-hand side boundary.

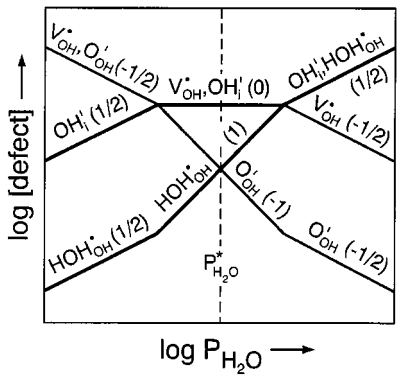

FIG. 3. Defect chemistry in hydroxides sketched as a function of water partial pressure based on the reactions described by Eqs. [2], [4], and [5] assuming $K_{(5)} \gg K_{(2)}$.

proton mobilities involving transfer from OH^- to O^{2-} are different from H_2O to OH^- by many orders of magnitude.

Below we shall see in detail that the conductivity always increases with water content leading to the assumption that water is essentially incorporated via reaction Eq. [4] and the intrinsic value, $[H_2O]^*$ corresponding to $P^*_{H_2O}$, in Fig. 2 is close to the $NaOH/Na_2O$ boundary. This is in agreement with the fact that the structure is fairly loose (7, 10–17).

Of considerable influence are carbonate impurities which we shall consider to be introduced as $(CO_3)'_{OH}$ according to

$$CO_2 + 2OH_{OH} \rightleftharpoons (CO_3)'_{OH} + H_2O^{\bullet}_{OH}. \qquad [8]$$

The formation of $H_2O^{\bullet}_{OH}$ is expected to lead to an increase in the proton conductivity as observed experimentally. In line with the above statements an increase of the proton conductivity upon CO_2 treatment is observed. Figure 4 displays the CO_2 effect. The right-hand side figures refer to a water excess situation while the left-hand side figures refer to a composition very close to the intrinsic value. The top figures are calculated by assuming equilibration with the gas phase while the bottom figures reflect a doped situation in which a certain CO_3^{2-} content has been introduced during preparation acting as a constant doping concentration at the temperatures of measurement. This difference affects the slopes in the regime of significant CO_3^{2-} content.

It is of course expected but worth mentioning that also the concentration of $V^{\bullet}_{OH}$ increases steeply (see Fig. 4) as illustrated by the reaction (coupling with reactions [5] and [4])

$$CO_2 + 2OH^{\times}_{OH} \rightleftharpoons (CO_3)'_{OH} + H_2O + V^{\bullet}_{OH}. \qquad [9]$$

The fact that both CO_2 and H_2O introduction lead to an increase of the conductivity but are antagonistic in terms of $V^{\bullet}_{OH}$ and OH'_i defects rules out that the proton transport is due to OH^- hopping.

PREPARATION AND CHARACTERIZATION

Several preparation procedures have been employed; see Ref. (9, 18). The technique used for obtaining essentially carbonate-free NaOH samples was sublimation in a CO_2-free environment. Owing to the marked hygroscopicity, high-vacuum treatment was not sufficient to keep the hydroxide water free. This was achieved by admixtures of Na_2O (see Fig. 5). For the transport measurements a small excess of Na_2O was deliberately introduced to establish a minimum water content which was checked by DSC experiments. Increasing the water content to a solubility limit of $\sim 2\%$ in the cubic phase depresses the melting point from 566 K to 561 K as displayed in Fig. 6. The absence of an impurity peak indicates a CO_2 content lower than 0.15 mol% (18, 19). Hence CO_2 effects are not expected to influence the proton conductivity of "wet NaOH" but may still be of relevance for the behavior of "dry NaOH." As already mentioned EPR analysis proved the absence of paramagnetic impurities ($\leq 10^{12}$ spins/cm^3).

CONDUCTIVITY AND PFG-NMR EXPERIMENTS: EXPERIMENTAL

Details of the experimental procedure and the apparatus are given in Refs. (9, 18) with respect to the impedance and NMR experiments. A typical impedance spectrum is shown

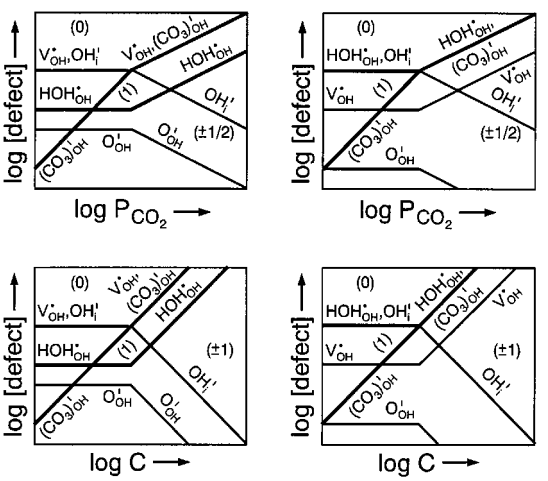

FIG. 4. The CO_2 effect on the defect chemistry in hydroxides based on Eqs. [2], [4], [5], and [8]. Upper row calculated for reversible CO_2 exchange, lower row for a fixed CO_2 content (termed C). Left-hand side columns and right-hand side column refer to different native situations (viz. center regime of FIG. 3 and right-hand side of Fig. 3, respectively.)

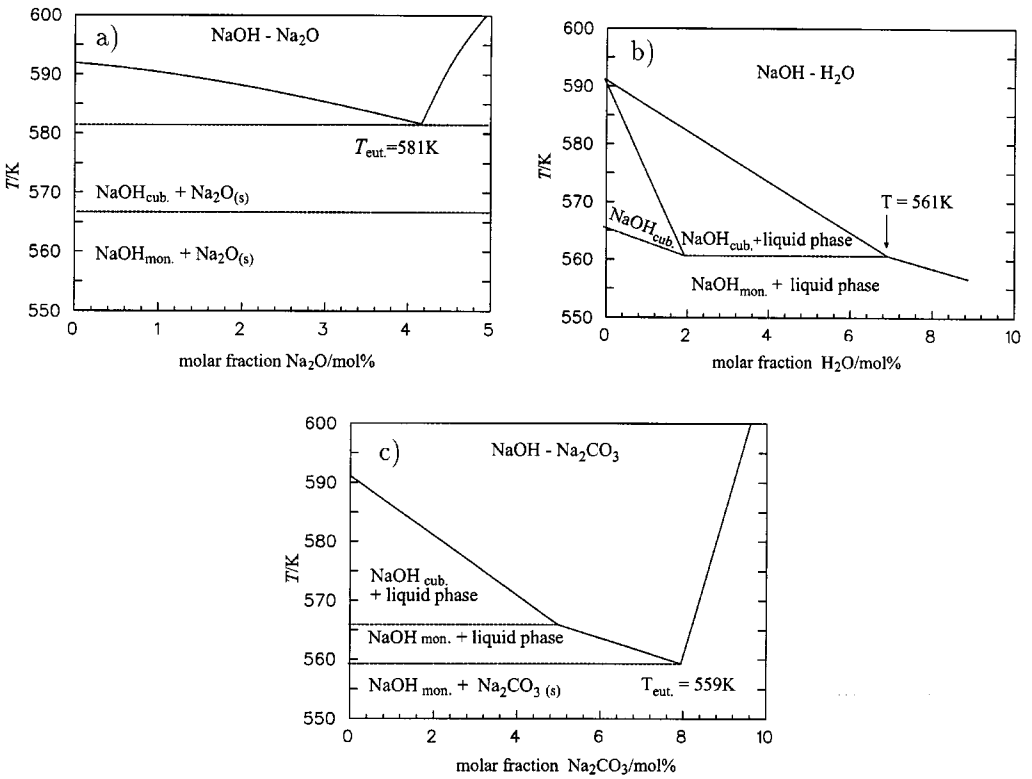

FIG. 5. Relevant diagrams (a) NaOH–Na_2O (21), (b) NaOH–H_2O (22), (c) NaOH–Na_2CO_3 (22).

in Fig. 7 (the exponent of the constant phase element of a simple R–Q circuit $\simeq 0.7$–0.9). The typical depression of the maximum frequency points toward correlation effects. In any experiment not even an indication of a deconvolution into separate semicircles was observed. In order to study the frequency effects more carefully microwave experiments have been performed.

Within a glove box NaOH powder was pressed into rectangular waveguide sections. To prevent corrosion, the stainless steel waveguide sections had been coated with a gold layer of 5 μm thickness. This sample holder was flanged to a microwave setup described elsewhere (23, 24). During the measurements the rectangular waveguide system was continuously flooded with dry Ar gas of high purity (99.999%). The complex conductivity was calculated from the experimentally determined attenuation of the transmitted and the reflected wave using a simulation method described elsewhere (23, 24).

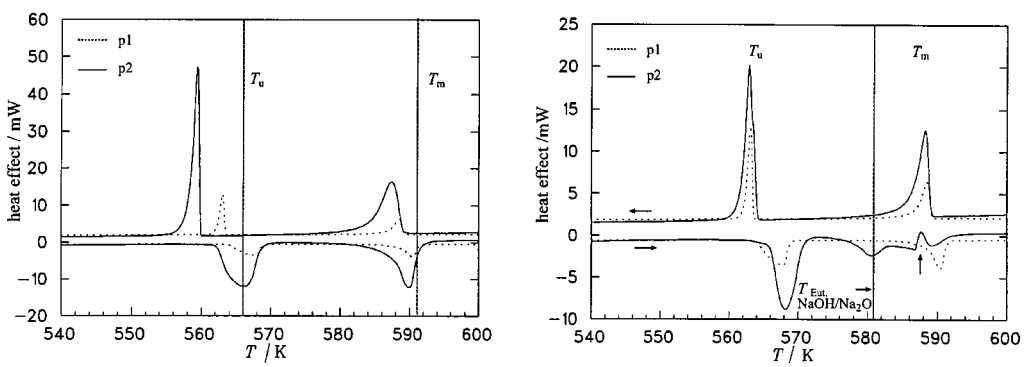

FIG. 6. Effects of H_2O and Na_2O on the transition points in NaOH according to DSC experiments (18) (left-hand side reflects the influence of different water contents; right-hand side: bottom curve shows the reaction of Na_2O excess with H_2O during heating, top curve corresponds to cooling of the water-free product. p1: $<1\%$ H_2O; p2: $\sim 3\%$ H_2O).

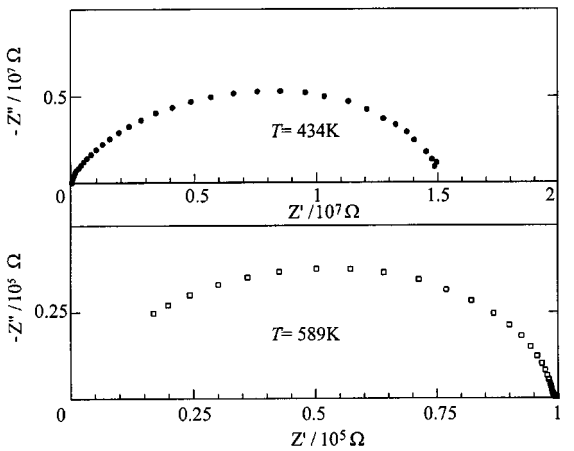

FIG. 7. Typical impedance spectra of NaOH sample (top, monoclinic; bottom, cubic).

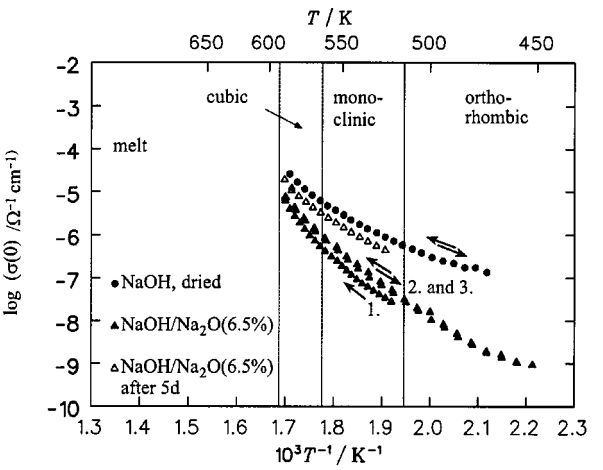

FIG. 9. (d.c.) conductivity derived from impedance measurements as a function of temperature.

CONDUCTIVITY AND NMR EXPERIMENTS: RESULTS

Conductivity Spectroscopy

Figure 8 shows the angular frequency dependence of $\sigma'(\nu)T$ obtained by impedance spectroscopy at various temperatures. σ' represents the real part of the complex conductivity (complex specific admittance). The low-frequency plateau reflects the d.c. conductivity values, in the following denoted by $\sigma(0)$ or simply by σ. The dashed straight line in Fig. 8 connects the angular frequencies ν_2, where the transition from the d.c. into dispersive regime for each isotherm occurs, ν_2 is defined by $\sigma'(\nu_2) = 2 \cdot \sigma(0)$.

The spectra are well-reproduced by forward–backward correlation effects described in the jump relaxation model (25). According to this model, all jumps not proven unsuccessful within the time window given by the inverse angular frequency do contribute to the conductivity. It is, therefore, found to increase with frequency.

Figure 9 displays the d.c. conductivity as a function of temperature for a nominally dry sample and a sample with a slight Na_2O excess. The conductivity decrease is definitely due to a lower H_2O content and not to a potential blocking by the second phase as studied in detail in Ref. (18). The values are much lower than reported previously in the literature. These literature values can be attributed to native (H_2O) and/or impurity effects (CO_2). The conductivity data have been rescaled using a scaling procedure proposed by Roling *et al.* (26). The results are shown in Fig. 10. Note that in contrast to Ref. (26) a semilogarithmic representation has been chosen. The scaled data of the cubic phase on the one hand and the data of the monoclinic/orthorhombic phase on the other hand form a master curve. The shift of the two master curves on the normalized frequency scale can either be traced back to different number densities of the mobile ions, different jump distances, or different Haven ratios existing in the various phases of NaOH.

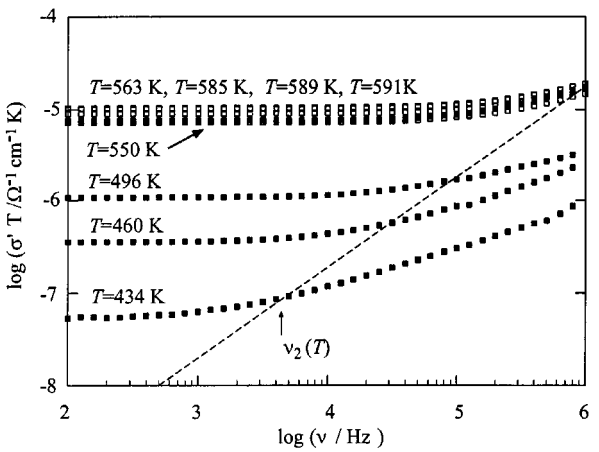

FIG. 8. Frequency dependence of the real part of the complex conductivity at different temperatures (filled symbols; monoclinic; open symbols, cubic NaOH).

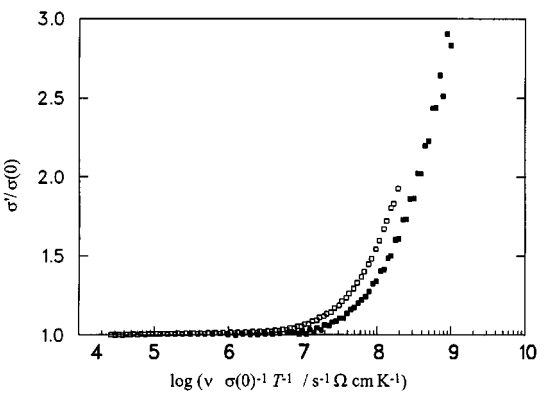

FIG. 10. Master curves according to Ref. (26) (see text).

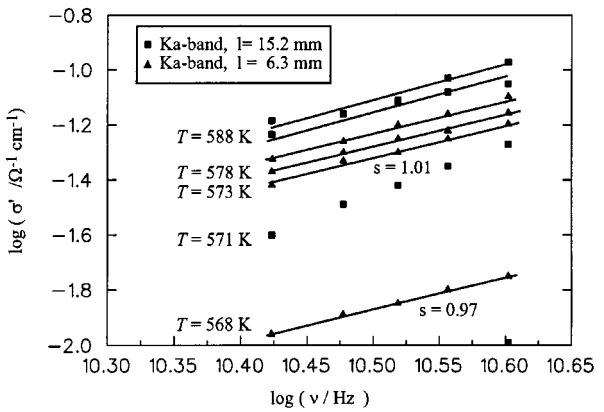

FIG. 11. Real part of the complex conductivity for high frequencies.

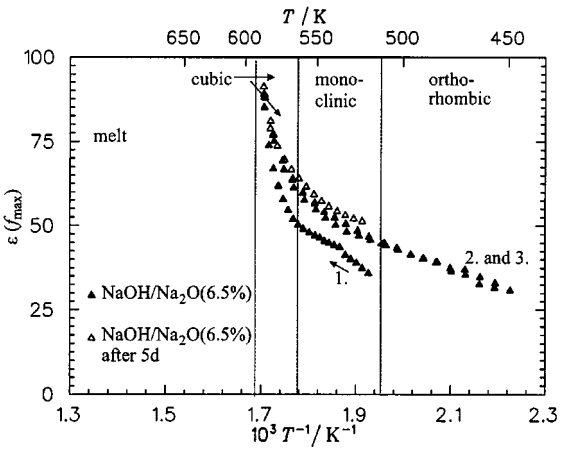

FIG. 13. Apparent dielectric constant derived from the maximum frequency of the impedance plots for various temperatures.

The fact that master curves can be constructed from the NaOH conductivity spectra confirms the validity of the time/temperature superposition principle for these data. It also indicates that in each phase the number density of the mobile ions does not significantly depend on temperature. This is in contrast to other crystalline ion conductors, such as AgBr (27) and β-AgI (28) for which the above-mentioned scaling procedure cannot be performed (29).

According to Ref. (30), $\sigma'(\nu)/\sigma(0)$ increases more rapidly when the normalized frequency is increased. The slope in a log–log plot of $\sigma'/\sigma(0)$ versus $\nu/(\sigma(0)T)$ finally attains unity. A slope of approximately one is clearly visible in the conductivity data of NaOH obtained by microwave measurements; see Fig. 11.

In Fig. 12 the real part of the complex conductivity at 33 GHz is shown as a function of temperature. σ' is significantly higher than $\sigma(0)$ since at high frequencies also translational ionic processes are observed which do not lead to successful hops; the increase from the monoclinic to the cubic phase is also noteworthy (not seen in Fig. 9).

Figure 13 gives the apparent dielectric constant derived from the maximum frequency of the impedance plots according to $((R^{1-n}Q)^{1/n})$ (31, 32) (n, exponent; R, Ohmic resistance; Q, frequency dependent capacitance). The high-frequency value of the real part of the complex permittivity could be reliably determined from the microwave measurements. It is only slightly frequency dependent and increases significantly at the transition from the monoclinic to the cube phase which is understandable in view of the dynamic rotational disorder (Fig. 14). Again such a sharp transition is not observed in the data at lower frequencies (see Fig. 13).

PFG-NMR

As observed from Fig. 15 diffusion coefficients derived from PFG-NMR are distinctly higher for dry NaOH than

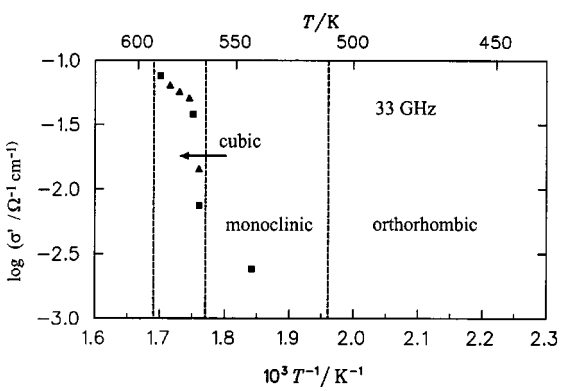

FIG. 12. Real part of the complex conductivity at 33 GHz as a function of temperature.

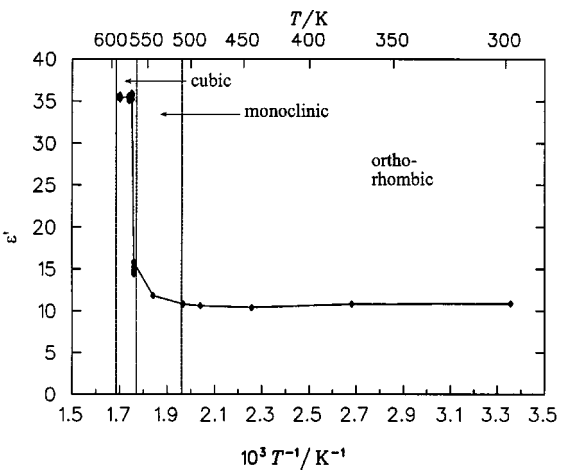

FIG. 14. Real part of the complex permittivity (high-frequency value) as a function of temperature.

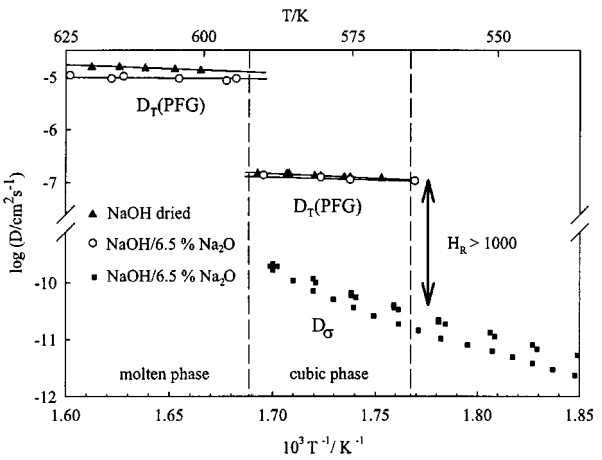

FIG. 15. PGF-NMR diffusion coefficients for differently dried NaOH (cf. Fig. 6). The distinctly lower large diffusion coefficients correspond to extremely high Haven ratios (H_R).

derived from d.c. conductivity. (No portions of molten phase could be detected.) The difference between dried NaOH with and without Na_2O excess in the cubic phase is less significant than for the conductivity. (Interestingly the molten phase reacts more sensitively with respect to H_2O traces. The monohydrate exhibits also comparatively high D values. The high values observed for NaOH containing an excess of $NaOH \cdot H_2O$ is due to melting point depression (18).) The fact that the data is higher than for the molten dry NaOH reflects again the H_2O influence.

DISCUSSION

Charge Transport

As far as the d.c. conductivity data (Fig. 16) is concerned, the discrepancy to the literature is striking. The values by Élk'kin *et al.* and especially by Haas *et al.* are greater by orders of magnitude. The disappearance of any jump at the nominal melting point indicates the formation of a liquid mixed phase involving a significant fraction of carbonate and/or water in the literature measurements. In fact Haas *et al.* (2) referred to the formation of eutectic OH^-/CO_3^{2-} melts, the transition point of which is further depressed by water. It is noteworthy that their values for the melt are higher than observed here, again pointing toward the role of H_2O/CO_2 with respect to the transport also in the liquid phase. The low values observed here can be attributed to the low H_2O/CO_2 content. The much decreased absolute value suggests transport via $H_2O^{\bullet}_{OH}$. In the water-rich regime we expect (u, mobility; $K_{(i)}$ refers to Eq. [i]).

$$\sigma_{H^+} \propto u_{H_2O^{\bullet}_{OH}} \cdot P_{H_2O}^{1/2} K_{(4)}^{1/2}, \qquad [10]$$

while around the intrinsic point (assuming $[OH_i'] \simeq [V^{\bullet}_{OH}]$)

$$\sigma_{H^+} \propto u_{H_2O^{\bullet}_{OH}} \cdot P_{H_2O} K_{(4)}^{1}. \qquad [11]$$

Exactly at the intrinsic point ($[H_2O^{\bullet}_{OH}] = [O'_{OH}]$) we could also write (assuming $u_{H_2O^{\bullet}_{OH}} \gg u_{O'_{OH}}$)

$$\sigma_H^* \sim F u_{H_2O^{\bullet}_{OH}} K_{(2)}^{1/2}. \qquad [12]$$

Adopting a value of $K_{(2)} = 10^{-10}\,\mathrm{mol^2/dm^6}$ proposed by (33) the mobility would be $\sim 10^{-5}\,\mathrm{cm^2\,s^{-1}\,V^{-1}}$, a not unreasonable value.

Also the behavior at the transition from the monoclinic to the cubic phase is worth being discussed. Since proton conduction via $H_2O^{\bullet}_{OH}$ requires reorientation, the transition from a rotationally ordered to a rotationally disordered phase should be reflected in the conductivity. The continuous and curved increase of $\sigma(0)$ with temperature (in contrast to Fig. 12) may be explained by inhomogeneity or extrinsic effects (see above). Figure 17 gives diffusion coefficient values derived from impedance and microwave measurements and PFG-NMR. The dotted curve corresponds to a power law fit using an exponent of 1 which has been derived from Fig. 11; the dashed curve corresponds to a master curve constructed from conductivity data of glassy $AgI–AgPO_3$ (30). Both are adjusted with respect to the low-frequency data. Note that the low-frequency data do not well agree with a unity power law in a better resolution and the curves are only shown for the purpose of a first orientation.

Even though the decrease in σ on decreasing the H_2O content can fairly firmly be ascribed to a lower proton conduction, it cannot be excluded that the residual value observed is due to a Na^+ conductivity. This might be

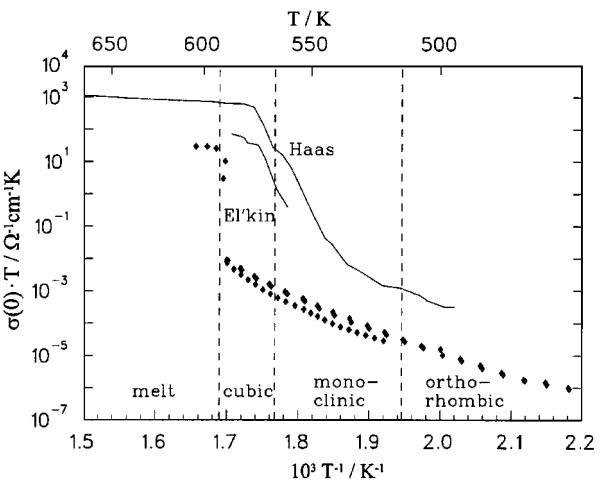

FIG. 16. Comparison of d.c. data with literature (6, 2).

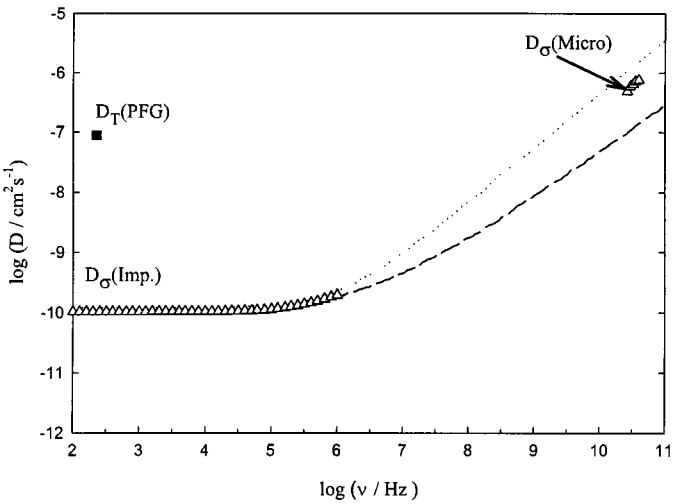

FIG. 17. Diffusion coefficients (cubic NaOH) derived from impedance spectroscopy, microwave experiments, and PFG-NMR. The dotted curve corresponds to a power law fit using an exponent of 1, the dashed curve to a master curve constructed from conductivity data of glassy AgI–$AgPO_3$; both adjusted with respect to the low frequency data.

supported by the fact that the activation enthalpy as well as the frequency behavior is quite comparable to that of NaCl. In that case the true Haven ratio could even be greater. These are, however, weak arguments and the fact that we did not observe electrode polarisation may favor H^+ conductivity. This is then also in line with the conclusion given in the previous section that the carrier density is T-independent pointing toward extrinsic protonic effects due to residual H_2O and/or CO_2 contents. Electronic contributions can be neglected according to the absence of redox-active ions, according to the EPR results and the fact that Na_2O_2 admixtures do not influence the electrical conduction (18).

Most striking is the huge discrepancy between NMR results and the diffusion coefficients converted from d.c. conductivity values via Nernst–Einstein equation D_σ. For the following discussion we shall neglect correlation effects of the order of unity. Then diffusion coefficients derived from PFG-NMR are equivalent to tracer diffusion coefficients (D^*). The values obtained for the cubic phase are as high as for high temperature phase of $CsHSO_4$, but must have a different origin (see above). Major differences between D^* and D_σ arise—generally speaking—if in addition to charged hydrogen motion also neutral transport is involved. As can be seen in Fig. 15, the ratio D^*/D_σ, commonly termed the Haven ratio, amounts at least to 10^4 while it falls down to ~ 1 in the liquid phase. If the conductivity in NaOH (cubic) partly stems from Na^+ motion, this is only the lower limit. The following mechanism is able to explain the giant Haven ratio: It assumes that there is cooperative proton motion extending to one or more faces of the $Na(OH)_{6/6}$ octahedra. As displayed in Fig. 18, the proton attached to O_B is transferred to O_C while H_A "jumps" to O_B and H_C to O_A. The back-mechanism may be avoided by the subsequent rotation of the proton around oxygen ($k_0 \simeq 10^{12}\,s^{-1}$ (13–15, 20)). This correlated circular exchange requires a special orientation; all OH groups have to point to each other as shown in Fig. 18. This "dance event" can also be continued over a longer range which is detected by PFG-NMR. The sheer existence of a correlated proton exchange has already been proposed in Ref. (13, 15) on the basis of neutron diffraction experiments.

Let us assess the entropy associated with a ring event.

$$\text{nil} \rightleftharpoons \text{ring event.} \qquad [13]$$

Neglecting vibrational entropy changes we have to calculate the remaining configurational entropy from statistics. Rather than to do this in a strict manner, it is sufficient for our purpose to correct the usual combinatorial expression

$$\left(\frac{N^*}{N}\right)$$

which counts the contribution of N^* (out of N possible) protons being in a right configuration, with the probability that this right configuration is involved in ring-dance. The latter factor is approximately $2/11^3$ (9). The factor of 2 stems from the number of possible configurations (clockwise and anticlockwise transition), the factor $(12-1)^3$ stems from the possibility to find three neighboring protons on a face of the $Na(OH)_{6/6}$ octahedron in the correct configuration. The oxygen to which the proton belongs has 12 neighbors. This number has to be corrected by 1 since two neighboring OH^- ions cannot point toward each other. Calculating from this a chemical potential we obtain

$$\mu = \Delta H^\circ - T\Delta S^\circ + RT \ln(N^*/N). \qquad [14]$$

ΔH° and ΔS° are the standard molar reaction enthalpy and entropy for the process under consideration (see

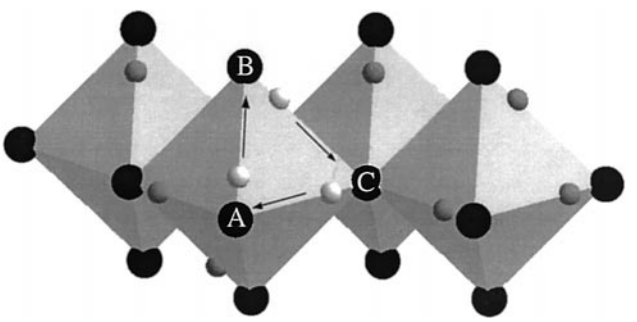

FIG. 18. Schematic representation of the model for correlated proton transport (9).

Eq. [13]). Since the chemical potential ($=\Delta G$) has to vanish in equilibrium (cf. reaction [13]) the concentration of the events [event] $\simeq N^*/N$ follows as

$$[\text{event}] = \exp\left(-\frac{\Delta H^\circ}{RT}\right)\exp\left(\frac{\Delta S^\circ}{R}\right). \qquad (15)$$

ΔS° is in the above approximation given by $R\ln(2/11^3)$. The self-diffusion coefficient is proportional to the diffusivity of a proton involved in the mechanism and to [event].

Ignoring migration entropies, we may derive ΔS° from the pre-factor of D^*. Assuming that jump distance $\simeq 5.1\sqrt{2}$ Å and attempt frequency $\omega_0 \simeq 10^{12}$/s, we estimate ΔS° to be $(-10 \ldots -20)$ J mol^{-1} K^{-1}, which may be compared to $R\ln 2/11^3 \simeq -50$ J mol^{-1} K^{-1}. It is important that both values are distinctly negative. The entropy values for KOH, RbOH, CsOH are indeed between $(-50$ and $-60)$ J mol^{-1} K^{-1} (9). The discrepancy in the case of NaOH can be easily explained by the above approximations, in particular by including ring exchange mechanisms extending over larger distances (probed by the measurements) and/or short-lived charge fluctuations. The latter would contribute to the microwave frequency and could even be able to explain the similar values of the tracer diffusion coefficient and the charge diffusion coefficient in the GHz regime. It would also explain in a natural way that the microwave data show a sharp effect at the transition from monoclinic to cubic phase (dance events) while the transition is smeared out in the d.c. conductivity (premelting of the "true" charge carriers).

CONCLUSIONS

The proton conductivity in NaOH is sensitively influenced by water and CO_2 content. The conductivity of very pure NaOH with minimum water content has a d.c. conductivity much lower than expected from the literature. The probable charge carrier is $HOH^{\bullet}_{OH}$ but also contribution from Na^+ cannot be ruled out in completely "dry" material. The tracer diffusion coefficient obtained by pulse field gradient NMR of the same samples are higher by at least 3 or 4 orders of magnitude than the tracer coefficient derived from the d.c. conductivity. Cooperative ring exchange mechanisms are proposed as an explanation with no or minor charge separation. Further measurements (NMR/neutron) are necessary to confirm this hypothesis.

ACKNOWLEDGMENTS

Discussions with Profs. K. Funke, H. Jacobs and Dr. B. Roling are gratefully acknowledged.

REFERENCES

1. W. Münch, K. D. Kreuer, U. Traub, and J. Maier, *J. Mol. Struct.* **381,** 1 (1996).
2. K.-H. Haas and U. Schindewolf, *J. Solid State Chem.* **54,** 342 (1984).
3. K.-H. Haas and U. Schindewolf, *Ber. Bunsenges. Phys. Chem.* **87,** 346 (1983).
4. M. S. Stephen and A. T. Howe, *Solid State Ionics* **1,** 461 (1980).
5. B. Sh. Élk'kin, E. K. Shalkowa, and Yu. M. Baikov, *Neorg. Mat.* **231,** 81 (1987).
6. B. Sh. Élk'kin, *Solid State Ionics* **37,** 139 (1990).
7. B. Mach and H. Jacobs, *Z. Anorg. allg. Chem.* **553,** 187 (1987).
8. H. Jacobs and B. Mach, *Z. Anorg. Chem.* **544,** 28 (1987); H. Jacobs, H. Jacobs and B. Harbrecht, *Z. Naturforsch. B* **36,** 270 (1981).
9. M. Spaeth, K. D. Kreuer, Th. Dippel, and J. Maier, *Solid State Ionics* **97,** 291 (1997).
10. B. Mach, Ph.D. thesis, Dortmund, Germany, 1984.
11. H. Jacobs, J. Kockelkorn, and Th. Tacke, *Z. Anorg. allg. Chem.* **531,** 119 (1985).
12. A. Giessler, G. Schaack, and H. Bleif, *Phys. Stat. Sol.* (*b*) **104,** 151 (1981).
13. U. Schotte, M. Kabs, H. Dachs, and K.-D. Schotte, *J. Phys. Condens. Matter* **4,** 9283 (1992).
14. K.-D. Schotte, U. Schotte, H.-J. Bleif, and R. Papoular, *Acta Crystallogr. A* **51,** 739 (1995).
15. U. Schotte, K.-D. Schotte, H. J. Bleif, M. Kabs, and H. Dachs, *J. Phys. Condens. Matter* **7,** 7453 (1995).
16. D. T. Amm, S. L. Segel, and K. R. Jeffrey, *Can. J. Phys.* **64,** 22 (1986).
17. H. D. Lutz, J. Henning, H. Jacobs, and B. Mach, *J. Mol. Structure* **145,** 277 (1986).
18. M. Spaeth, Ph.D. thesis, University of Stuttgart, Germany, 1997.
19. H.-J. Bleif, Ph.D. Thesis, Us 78.6786, University of Tübingen, Germany, 1978.
20. J. G. Smit, H. Dachs, and R. E. Lechner, *Solid State Commun.* **29,** 219 (1979).
21. R. Cohen-Adad and C. Ruby, *Compt. Rend. Acad. Bulg. Sci.* **258,** 6163 (1964).
22. R. Cohen-Adad, M. Michaud, J. Said, and A. P. Rollet, *B. Soc. Chim. France*, **2,** 356 (1961).
23. K. Funke, J. Kümpers, and J. Hermeling, *Z. Naturforsch. A* **43,** 1094 (1988).
24. R. Hoppe, T. Kloidt, and K. Funke, *Ber. Bunsenges. Phys. Chem.* **100,** 1497 (1996).
25. K. Funke, *Progr. Solid Stat. Chem.* **22,** 111 (1993).
26. B. Roling, A. Happe, K. Funke, and M. D. Ingram, *Phys. Rev. Lett.* **78,** 2160 (1997).
27. K. Funke, T. Lauxtermann, D. Wilmer, and S. M. Bennington, *Z. Naturforsch.* **50,** 509 (1995).
28. K. Funke, T. Lauxterman, D. Wilmer, R. Holzgreve, and S. M. Bennington, *Solid State Ionics* **86–88,** 141 (1996).
29. B. Roling, unpublished results.
30. K. Funke, B. Roling, and M. Lange, *Solid State Ionics* **105,** 195 (1998).
31. J. Jamnik, M. Gaberscek, and S. Pejovnik, *Electrochim. Acta.* **35,** 423 (1990).
32. G. V. Brug, A. L. G. van den Eden, M. Sluyters-Rehbach, and J. H. Sluyters, *J. Electroanal. Chem.* **176,** 275 (1984).
33. B. Tremillon and R. Doinseau, *J. Chim.* **71,** 1379 (1974).